npj | climate and atmospheric science

Article

Published in partnership with CECCR at King Abdulaziz University

https://doi.org/10.1038/s41612-026-01388-7

Atmospheric deposition and lateral ocean transport enhance nitrogen supply to the North Pacific Subtropical Gyre

Lunbi Wu[1,5], Dongchen Dai[1,5], Wentao Ma[2], Jin-Yu Terence Yang[1] ✉, Ziyang Zhang[2], Li Luo[3], Xin Liu[4], Hongyan Bao[1], Shuh-Ji Kao[3] & Minhan Dai[1]

Atmospheric nitrogen deposition is an important external nitrogen source to the ocean that can fuel export production, yet its origin and contribution remain uncertain in the nitrogen-limited North Pacific Subtropical Gyre (NPSG). We present aerosol nitrate and reduced nitrogen (RN) concentrations and nitrogen isotopic composition ($\delta^{15}N$), along with air-mass back trajectories, across the NPSG in summer and winter. High $\delta^{15}N$ values (–0.4‰ to 3‰) of aerosol nitrate and RN suggest that natural sources dominate in both seasons, contributing only modestly to the local external nitrogen supply. A synthesis of historical observations reveals pronounced zonal gradients in aerosol nitrogen concentrations and $\delta^{15}N$ between the NPSG and transition zone, indicating enhanced anthropogenic influence in the latter, where nitrogen limitation is weaker. We estimate that lateral ocean transport from the transition zone increases external nitrogen inputs to the NPSG by 18%, highlighting an indirect pathway linking human emissions to oligotrophic ocean productivity.

Nitrogen availability limits primary productivity and carbon sequestration in most of the ocean, thereby playing a pivotal role in regulating Earth's climate[1]. External (allochthonous) inputs of reactive nitrogen (N_r) to the ocean's sunlit surface can increase the marine nitrogen inventory and stimulate the biological carbon pump[2]. While biological N_2 fixation has traditionally been considered the dominant external nitrogen source in oligotrophic oceans[3], atmospheric N_r emissions have increased substantially over the past century due to human activities and can be transported rapidly to remote ocean basins[4]. Atmospheric nitrogen deposition (AND) is therefore now recognized as a significant pathway supplying bioavailable nitrogen to the surface ocean, with profound implications for marine biogeochemical cycles and global climate[5–7].

Oligotrophic subtropical gyres, including the North Pacific Subtropical Gyre (NPSG), are strongly N-limited[8] and thus highly sensitive to external N_r supply[1]. Over recent decades, the western North Pacific (wNP) has experienced substantial increases in anthropogenic nitrogen fluxes originating from East and South Asia[9,10]. Model simulations indicate that AND fluxes are considerably high along the Asian continental margin and in open-ocean regions downwind of the continent, decreasing sharply toward the NPSG[2]. However, ocean circulation processes associated with western boundary currents, including mesoscale eddies, Ekman transport, and enhanced mixing, can contribute to the cross-frontal exchange of nutrients between the subpolar and subtropical gyres[11,12]. Such lateral transport may deliver external nitrogen into the NPSG interior, potentially amplifying the influence of anthropogenic emissions beyond areas of direct atmospheric deposition. Observational constraints on these processes, however, remain limited.

Field observations of atmospheric aerosol nitrogen in the wNP have been sparse, focusing mainly on its marginal seas and mid- to high-latitude open-ocean regions, where anthropogenic nitrogen emissions are high[13–16]. However, some observations indicate that aerosol nitrate and ammonium concentrations in the western NPSG can be comparable to those in more polluted regions[17–20]. Atmospheric organic nitrogen measurements are even scarcer, despite evidence that this component may constitute a substantial fraction of atmospheric N_r over the open ocean[14,20,21]. Seasonal variability in aerosol nitrogen is also poorly characterized owing to insufficient wintertime measurements, yet models indicate elevated AND fluxes during boreal winter[22]. In this context, the magnitude, distribution, and sources of atmospheric N_r over the wNP and its contribution to the surface-water nitrogen budget remain highly uncertain.

Stable nitrogen isotopes ($\delta^{15}N$) provide a powerful framework for distinguishing between anthropogenic and natural sources of aerosol N_r in

[1]State Key Laboratory of Marine Environmental Science, College of Ocean and Earth Sciences, Xiamen University, Xiamen, China. [2]State Key Laboratory of Satellite Ocean Environment Dynamics, Second Institute of Oceanography, Ministry of Natural Resources, Hangzhou, China. [3]State Key Laboratory of Marine Resource Utilization in South China Sea, Hainan University, Haikou, China. [4]State Key Laboratory of Marine Environmental Science, College of the Environment and Ecology, Xiamen University, Xiamen, China. [5]These authors contributed equally: Lunbi Wu, Dongchen Dai. ✉e-mail: jyyang@xmu.edu.cn

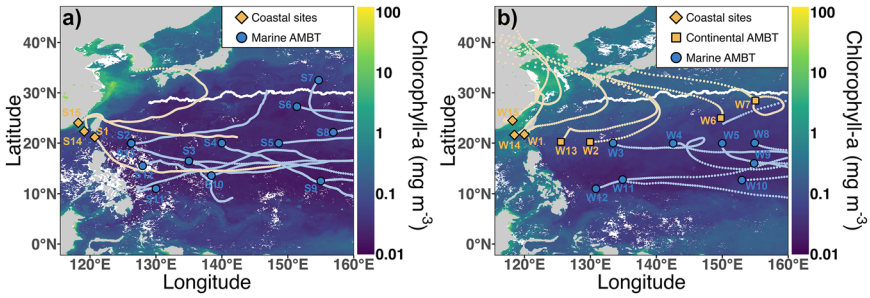

Fig. 1 | Aerosol sampling end locations and surface chlorophyll-a (Chl-a) concentrations in the western North Pacific during the summer and winter cruises. **a** for the summer cruise, **b** for the winter cruise. The white curve represents the boundary between the NPSG and the transition zone (NPTZ) in the western North Pacific (0-50°N; 122°E-160°E)[8]. The distribution of surface Chl-a obtained from MODIS-Aqua (https://www.oceancolour.org/) is shown as monthly averages for the aerosol sampling periods: June-August 2020 (summer) and December 2020 to February 2021 (winter). The 7-day air mass backward trajectories (AMBTs; dotted lines) for starting altitudes of 500 m above ground level are connected to the sampling end locations (see "Methods"). The AMBTs at sites within the NPSG that traversed or passed over the continent were classified as continental AMBTs (orange). In contrast, those originating from the remote open ocean to the east were classified as marine AMBTs (light blue).

remote oceanic regions[23]. Aerosol nitrate from anthropogenic/terrestrial emissions typically exhibits lower δ^{15}N-NO_3^- values than nitrate from natural sources[18,24–28]. However, recent observations reveal that marine alkyl nitrates emitted from the ocean surface can also produce isotopically light aerosol nitrate[29], complicating source attribution. Isotope constraints on aerosol ammonium and organic nitrogen over the open ocean are particularly limited. Available evidence suggests that, compared to terrestrial sources, marine emissions contribute substantially to aerosol ammonium with lower δ^{15}N values, at least over the Atlantic Ocean[30,31]. By comparison, aerosol organic nitrogen, derived mainly from marine biogenic sources, may exhibit positive δ^{15}N values[32,33]. To date, the sources of atmospheric N_r over the NPSG have not been adequately validated, underscoring the need for comprehensive measurements of multiple N_r species.

In this study, we conducted aerosol sampling over the oligotrophic NPSG during both summer and winter (Fig. 1 and Supplementary Table S1) to characterize the concentrations and δ^{15}N of major aerosol N_r species and to constrain their dominant sources in each season. By integrating these observations with historical datasets across the wNP, we assessed region-scale patterns in aerosol N_r sources and their contributions to the marine nitrogen budget. We further evaluated the role of lateral ocean transport in redistributing external nitrogen inputs to the NPSG on seasonal and annual timescales.

Results

Concentrations of water-soluble Nr species in aerosols over the NPSG

During the summer cruise, air mass backward trajectories (AMBTs) at sites near China's southeastern coast (sites S14, S15, and S1) traversed or passed over the continent and were therefore classified as continental AMBTs. In contrast, AMBTs at sites within the NPSG predominantly originated from the remote open ocean to the east and were classified as marine AMBTs (Fig. 1; Supplementary Table S2). Despite substantial variability, concentrations of all water-soluble N_r species in marine aerosols with continental AMBTs were markedly higher than those with marine AMBTs (Fig. 2; Supplementary Fig. S1 and Table S3). Over the western NPSG, concentrations of water-soluble N_r species exhibited relatively limited spatial variability. During summer, NO_3^- dominated the WSTN pool, accounting for 44.8-91.5% of WSTN, with a mean contribution of 64.2% (Supplementary Fig. S2).

During the winter cruise, air masses influencing the western and northern sites within the NPSG (W2, W13, W6, and W7), as well as the coastal sites, originated over or near the continent, whereas sites east of 130°E in the central NPSG were mainly influenced by air masses from the open ocean (Fig. 1b). Spatially, higher concentrations of water-soluble N_r species were observed at the coastal sites and at the western NPSG sites with continental AMBTs. In contrast, among the remaining open-ocean sites, concentrations of water-soluble N_r species did not differ substantially between sites with continental AMBTs in the northern NPSG and those with marine AMBTs in the central NPSG (Fig. 2). Compared with summer conditions, coastal sites with continental AMBTs had higher concentrations of all water-soluble N_r species during winter (Fig. 2; Supplementary Fig. S2). At open-ocean sites with marine AMBTs, wintertime concentrations of WSTN (5.29 ± 2.17 nmol m^{-3}), NH_4^+ (1.74 ± 1.05 nmol m^{-3}), and WSON (2.05 ± 2.30 nmol m^{-3}) were higher than those in summer, whereas NO_3^- concentrations (1.50 ± 0.34 nmol m^{-3}) were comparable between seasons (Supplementary Figs. S1 and S2). Throughout the winter cruise, WSTN exhibited a balanced composition, with similar contributions from NO_3^-, NH_4^+, and WSON (Supplementary Fig. S2).

Isotopic composition of water-soluble Nr species in aerosols over the NPSG

Figure 3 presents the δ^{15}N values of aerosol NO_3^-, RN, and WSTN over the NPSG during the summer and winter cruises. Overall, the δ^{15}N-RN values exhibited a wider range (−3.0‰ to 12.6‰) than δ^{15}N-NO_3^- (−3.6‰ to 4.8‰) and δ^{15}N-WSTN (−2.8‰ to 6.3‰) (Supplementary Table S3). For both seasons, the δ^{15}N values of aerosol N_r species differed markedly between samples with continental and marine AMBTs.

During summer, most aerosol samples with either continental AMBTs or marine AMBTs displayed positive δ^{15}N values for the water-soluble N_r species (Fig. 3). The concentration-weighted δ^{15}N values of NO_3^- (1.0‰ vs. 2.2‰), RN (2.3‰ vs. 6.8‰), and WSTN (1.5‰ vs. 4.4‰) in aerosols with marine AMBTs were consistently lower than those with continental AMBTs. In addition, the δ^{15}N values of the water-soluble N_r species in aerosols with marine AMBTs exhibited less variability. One exception was the sample collected at S9 (155°E, 12°N), which contained negligible WSON and showed an anomalously high δ^{15}N-RN value (12.6‰).

In winter, the δ^{15}N values of water-soluble N_r species were generally lower than those observed in summer, particularly for NO_3^- (Fig. 3). The wintertime δ^{15}N-NO_3^- values were significantly lower than the δ^{15}N-RN values (Fig. 3). As in summer, the concentration-weighted δ^{15}N-NO_3^- value was lower in aerosols with marine AMBTs than with continental AMBTs (−0.4‰ vs. 1.9‰). Aerosol NO_3^- with marine AMBTs also showed a lower concentration-weighted δ^{15}N value in winter than in summer. In contrast, the wintertime concentration-weighted δ^{15}N values of RN (3.3‰ vs. −0.5‰) and WSTN (2.1‰ vs. 0.6‰) were higher in aerosols with marine AMBTs than in those with continental AMBTs. Compared with summer observations, wintertime aerosol with continental AMBTs showed lower concentration-weighted δ^{15}N values for RN and WSTN, whereas that with marine AMBTs exhibited slightly higher concentration-weighted δ^{15}N values.

Discussion

At the coastal sites, aerosol NO_3^- and RN with continental AMBTs displayed higher concentrations that were one to two orders of magnitude

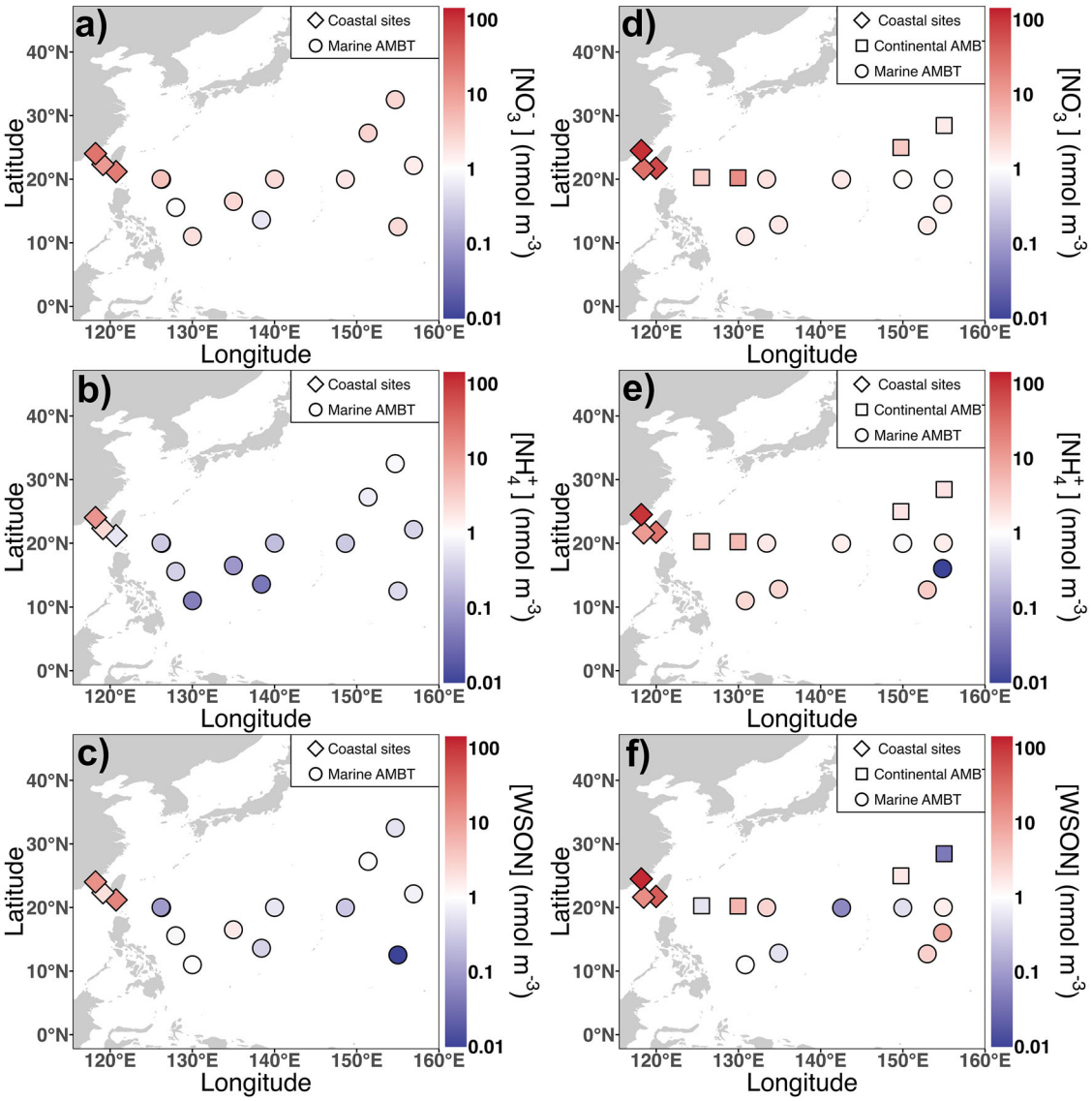

Fig. 2 | Concentrations of water-soluble N_r species in aerosols collected over the NPSG during the summer and winter cruises. a–c show NO_3^-, NH_4^+, and WSON, respectively, for the summer cruise, while **d–f** present the corresponding species for the winter cruise.

higher than those observed at the open-ocean sites in the NPSG for both seasons. These aerosols exhibited distinct $\delta^{15}N$ values compared to samples with marine AMBTs (Fig. 3), indicating contrasting source regimes between coastal and remote regions. Before reaching the coastal sites, air masses passed over the densely populated regions of East Asia (Fig. 1), where anthropogenic N_r emissions rank among the highest globally[34]. As observed previously along the northwestern Pacific margins[35–37], these concentrations and isotopic characteristics indicate that aerosol NO_3^- and RN at coastal sites with continental AMBTs are predominantly derived from anthropogenic and terrestrial sources.

In contrast to the coastal sites, air masses over most open-ocean sites originated from the remote regions of the North Pacific and did not traverse East Asia during either season (Fig. 1). Aerosol NO_3^- and RN concentrations declined sharply offshore, suggesting efficient removal of anthropogenic N_r from the marginal seas. Consequently, aerosol NO_3^- and RN over the NPSG are likely dominated by non-terrestrial sources and in situ marine processes.

The concentration-weighted average $\delta^{15}N\text{-}NO_3^-$ values with marine AMBTs (1.0‰ in summer and −0.4‰ in winter; Fig. 3) are comparable to previous observations in remote oceanic regions[27] and point to a dominant contribution from lightning-derived NO_x to aerosol NO_3^- [23,25]. In addition, the $\delta^{18}O\text{-}NO_3^-$ values showed limited seasonal fluctuations (33.36 ± 7.83‰; Supplementary Table S3) and were substantially lower than those associated with ozone oxidation pathways, which typically occur in polluted areas with higher ozone concentrations[38]. This also suggests that aerosol NO_3^- over the NPSG is largely produced by localized sources and by reaction with the hydroxyl radical in the marine boundary layer[19], rather than by long-range transport from polluted regions. Nevertheless, moderately elevated $\delta^{15}N\text{-}NO_3^-$ values (reaching 4.4‰) observed in several summer samples likely reflect hemisphere-scale transport of continental-sourced peroxyacetyl nitrate (PAN) and subsequent NOx release over the subtropical regions[24], as supported by model simulations[39]. The visible seasonal differences in $\delta^{15}N\text{-}NO_3^-$ values are unlikely to be driven by changes in lightning NOx production, which exhibit minimal seasonality in the tropics[40]. Instead, isotope fractionation during gas-particle partitioning during heterogeneous halogen chemistry in the marine boundary layer, which preferentially incorporates ^{15}N into particulate nitrate[24], provides a more plausible explanation. Enhanced sea-salt aerosol production (including Na^+ and Cl^-) under stronger winter winds may amplify this process, consistent with the frequent occurrence of negative $\delta^{15}N\text{-}NO_3^-$ values (Fig. 1; Supplementary Table S3).

This isotope fractionation was particularly evident in continentally influenced air masses reaching the open-ocean sites during winter, where

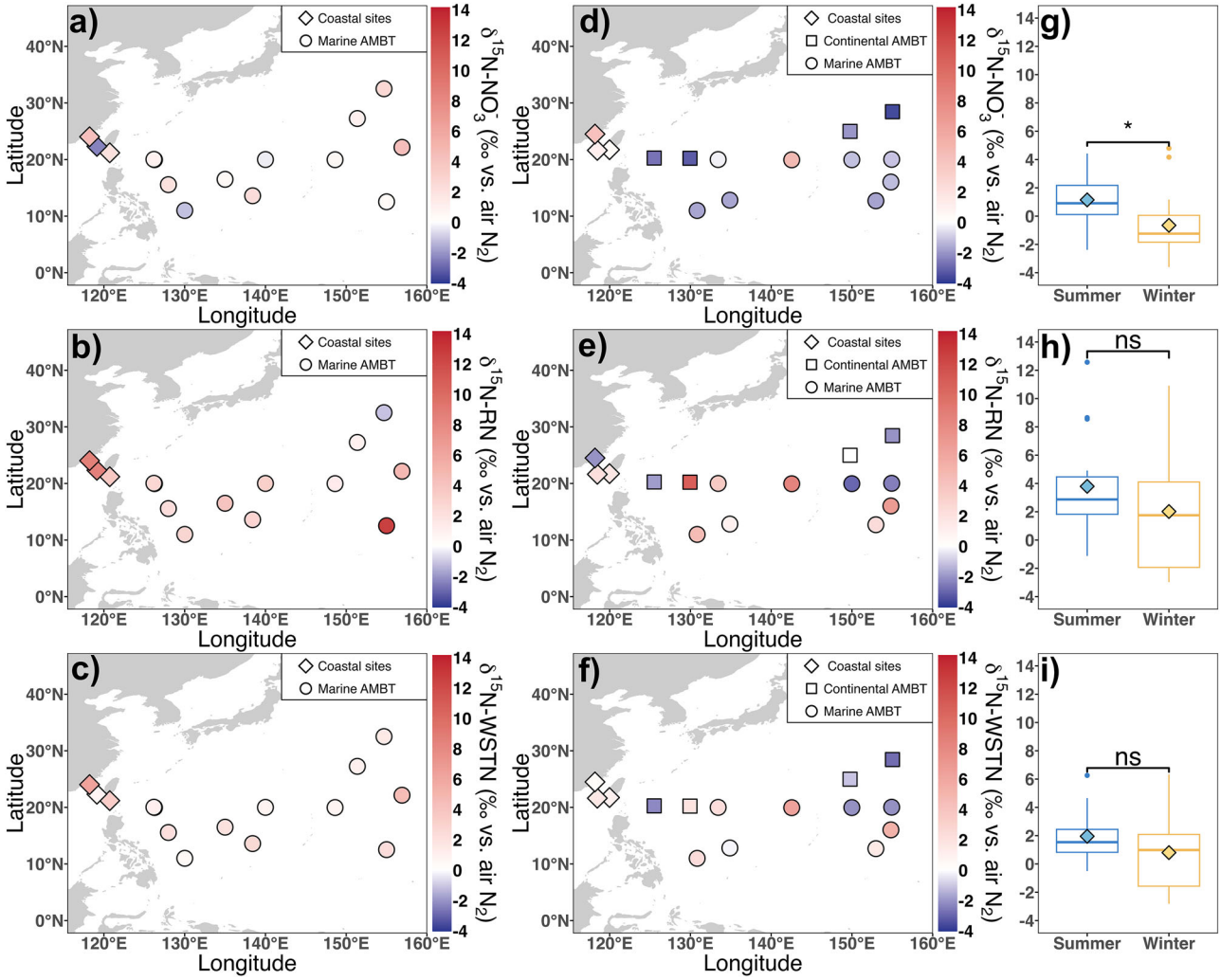

Fig. 3 | N isotope composition (‰ vs. air N_2) of water-soluble N_r species in aerosols collected over the NPSG during the summer and winter cruises. a–c show NO_3^-, reduced nitrogen (RN), and WSTN, respectively, for the summer cruise, while **d–f** present the corresponding species for the winter cruise. The box-and-whisker plots show seasonal comparisons of the N isotope composition of NO_3^- (**g**), RN (**h**), and WSTN (**i**) observed over open-ocean sites of the NPSG. The line and diamond symbol in the plot denote the median and mean, respectively.

aerosol NO_3^- concentrations and their $\delta^{15}N$ values (less than −2.5‰) were markedly lower than those at the coastal sites (Fig. 1; Supplementary Fig. S3a). Such offshore patterns are consistent with progressive removal of ^{15}N-enriched particulate nitrate during long-range transport, a feature widely observed from coastal to remote oceanic regions[24]. The strong relationship between $\delta^{15}N$-NO_3^- and the logarithm of NO_3^- concentrations ($p < 0.01$, $R^2 = 0.61$; Supplementary Fig. S3a) suggests the importance of transport-related chemistry in shaping $\delta^{15}N$-NO_3^- over the open ocean. This finding underscores the need to explicitly account for atmospheric processing when attributing aerosol NO_3^- sources in remote oceanic environments.

Unlike marine aerosol NO_3^-, marine aerosol RN exhibits more complex source characteristics, as reflected by the wide variability in NH_4^+/RN ratios and $\delta^{15}N$-RN (Fig. 3; Supplementary Fig. S3b). The persistently low concentrations of aerosol NH_4^+ and WSON with marine AMBTs, together with their short atmospheric lifetimes (typically less than a few days[23]), indicate that local marine emissions, rather than anthropogenic sources, dominate the atmospheric RN pool over the NPSG in both seasons. This inference is supported by the strong positive correlation between aerosol NH_4^+ concentration and wind speed (Supplementary Fig. S4), consistent with the understanding that enhanced sea-air NH_4^+ exchange occurs under high-wind conditions[30]. Similarly, aerosol WSON concentrations were higher in winter, accompanied by elevated wind speeds and sea-salt Na^+ and Chl-a contents (Supplementary Tables S2 and S3), further pointing to a marine biological origin. These patterns agree with previous findings in the North Pacific and South Atlantic[20,21]. Additionally, recent evidence links aerosol WSON to N_2 fixation and marine DON, suggesting a potential contribution from diazotroph-derived N_r[41], which may be particularly plausible in the NPSG, where N_2 fixation rates are high[42,43].

Elemental and isotopic mixing analysis was examined to further constrain RN sources. Most samples fall within the range of marine NH_4^+ and organic nitrogen endmembers (Supplementary Fig. S3b). Samples with lower NH_4^+/RN ratios, reflecting a greater contribution of WSON, exhibited higher $\delta^{15}N$-RN values, pointing to the endmembers of seawater $\delta^{15}N$-DON and marine aerosol $\delta^{15}N$-ON. As the NH_4^+/RN ratio increased, the $\delta^{15}N$-RN values became more scattered and lower, consistent with the wide isotopic variability in marine NH_4^+ sources as previously reported in aerosols and rainwater[31,44]. Although the broad range of $\delta^{15}N$-NH_4^+ complicates precise source appointment, the combination of short lifetimes, remote air-mass origins, and isotopic characteristics strongly supports marine origins for aerosol NH_4^+ over the NPSG. Overall, these results demonstrate that oceanic emissions play an important role in shaping aerosol RN over the NPSG, challenging the traditional view of the ocean as a passive recipient of N_r deposition from land. Our findings align with recent

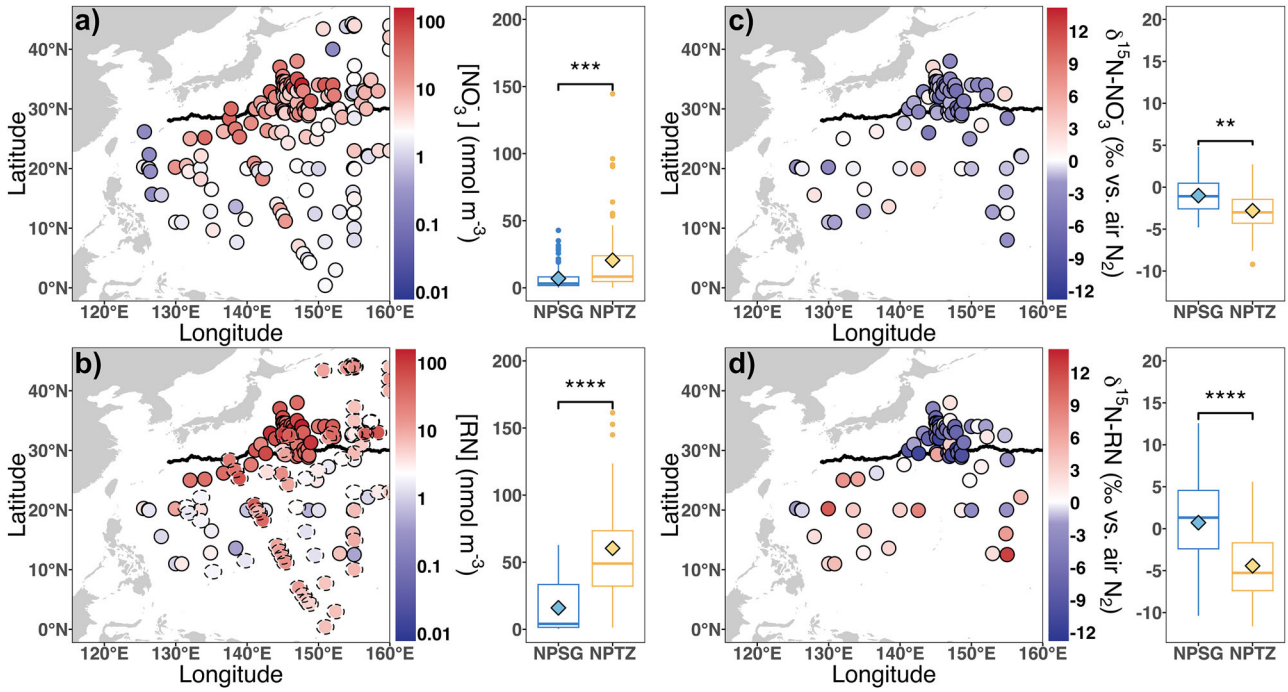

Fig. 4 | Concentrations and N isotope composition of NO_3^- and RN in aerosols over the western North Pacific. **a**, **c** for NO_3^-, and **b**, **d** for RN. The dashed dots in **b** indicate datasets lacking measurements of organic nitrogen; we assumed it to be 30% of total nitrogen, consistent with our measurements (Supplementary Fig. S2) and previous studies[2]. The solid curve represents the boundary between the NPSG and NPTZ[8]. The box-and-whisker plots show the data for the NPSG and NPTZ. The line and diamond symbol in the box plot denote the median and mean values, respectively. Data are compiled from Baker et al.[65], Kamezaki et al.[18], Luo et al.[14,33], Seok et al.[66], Shi et al.[27], and this study.

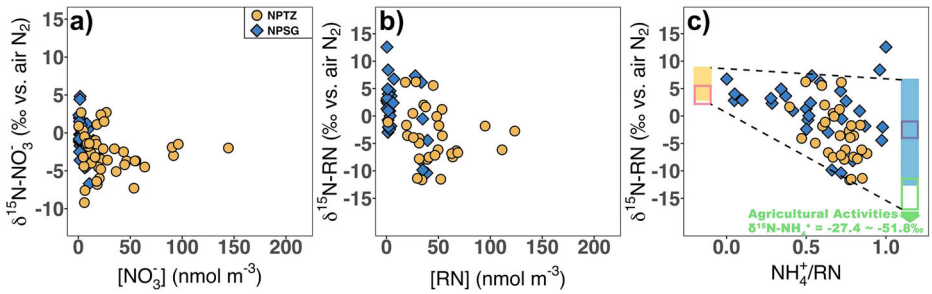

Fig. 5 | Scatter plots of N isotope composition versus concentrations of aerosol Nr between the NPSG and NPTZ in the western North Pacific. **a** for $\delta^{15}N$-NO_3^- versus NO_3^- concentration, **b** $\delta^{15}N$-RN versus RN concentration, and **c** NH_4^+/RN ratio between the NPSG and NPTZ in the western North Pacific. The green, purple, and blue bars in **c** denote the $\delta^{15}N$-NH_4^+ endmembers of vehicle emissions, surface seawater, and marine source aerosol. The green arrow in **c** indicates the $\delta^{15}N$-NH_4^+ endmember of agricultural activities in North China. The orange and pink bars in **c** show the $\delta^{15}N$ values of total nitrogen dominated by organic nitrogen in marine aerosols and the surface seawater $\delta^{15}N$-DON observed in the NPSG, respectively. The data are derived from those shown in Fig. 4.

observations from Bermuda in the North Atlantic, which indicate that marine processes constitute a significant source of atmospheric RN in remote oceanic regions[23].

To assess region-scale patterns in aerosol N_r sources, we integrated our new measurements with historical observations spanning all seasons to generate a comprehensive map of aerosol N_r concentrations and $\delta^{15}N$ signatures across the wNP (0-50°N, 122°E-160°E; Fig. 4; Supplementary Fig. S5). Coastal data (water depth shallower than 200 m) were excluded to minimize local influences. Based on different Chl-a levels and nutrient regimes, the study area was divided into the N-limited oligotrophic subtropical gyre (with Chl-a content < 0.1 mg m^{-3} and NO_3^- concentration < 0.4 μmol L^{-1}) and the non-N-limited mesotrophic transition zone (with Chl-a content > 0.1 mg m^{-3} and NO_3^- concentration > 0.4 μmol L^{-1}) (Supplementary Fig. S6).

Notable spatial gradients were observed in both concentrations and $\delta^{15}N$ values of aerosol NO_3^- and RN (as well as WSTN) across the wNP (Fig. 4; Supplementary Figs. S7 and S8). Concentrations of NO_3^-, NH_4^+, and WSON were significantly higher in the transition zone (NPTZ) and in the western part (< 150°E) of the North Pacific, reflecting proximity to continental sources (Supplementary Figs. S8 and S9). In parallel, the $\delta^{15}N$ values of aerosol NO_3^- and RN presented clear latitudinal gradients, with more ^{15}N-depleted signatures in the NPTZ than in the NPSG (Fig. 4). These spatial patterns were closely linked to AMBTs (Supplementary Figs. S5 and S10). Continental AMBTs were associated with higher N_r concentrations and lower $\delta^{15}N$ values, whereas marine AMBTs featured lower concentrations and higher $\delta^{15}N$ values. Therefore, aerosol N_r concentrations and isotope signals exhibit coherent distribution patterns that are consistent across air mass origins and geographical settings (Fig. 5; Supplementary Fig. S10).

In the NPTZ, higher concentrations and more negative $\delta^{15}N$ values of NO_3^- and RN in most aerosol samples with continental AMBTs indicate a significant influence of anthropogenic and continental N_r inputs from East Asia[2,17,33]. These results are consistent with previously documented observations of aerosol NO_3^- in downwind areas of polluted North America,

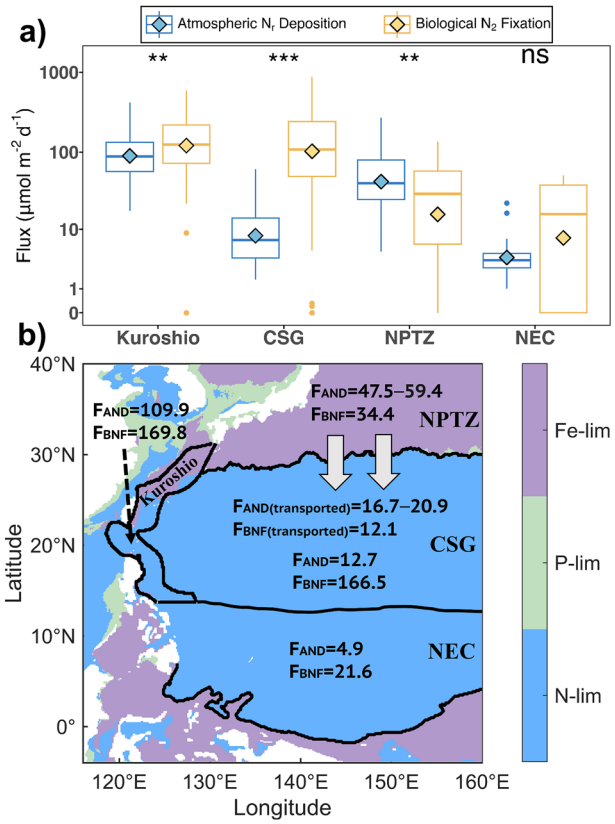

Fig. 6 | Spatial distribution of external nitrogen inputs across subregions of the western Pacific and estimated lateral transport fluxes from the NPTZ to the central subtropical gyre. a Box-and-whisker compilation of published observational datasets of net aerosol N_r and N_2 fixation fluxes across the subregions of the western North Pacific (see Supplementary Fig. S11). The line and diamond symbols in the box plot denote the median and mean values, respectively. The data on N_2 fixation fluxes are from Shao et al.[43] Sato et al.[67], and Yu et al.[68]. The Kuroshio aerosol N_r deposition fluxes are from Baker et al.[65] and Luo et al.[33]. **b** In situ fluxes of net aerosol N_r deposition and N_2 fixation (F_{AND} and F_{BNF}; μmol m^{-2} day^{-1}) in the subregions and their lateral transport fluxes from the NPTZ to the central subtropical gyre (CSG) via lateral ocean circulation above the mixed layer. Note that aerosol N_r deposition flux in the NPTZ and the associated transport estimates derived from the full dataset were treated as the lower bound, whereas those based solely on data with continental AMBTs were considered the upper bound (also see Supplementary Fig. S5, and Tables S4 and S5). The map's background colors represent nutrient limitation conditions for pico-phytoplankton, which is dominant in the study area.

Western Europe, and Southern China[24,28,45,46]. The dominance of NH_4^+ in aerosol RN, together with more negative δ^{15}N-RN values, points to the isotopic endmembers of vehicle and agricultural emissions (Fig. 5c), the major sources of NH_3 in North China[47]. Moreover, the mean ratio of NH_4^+ to NO_3^- in aerosols (~2) in the NPTZ aligns with the ratio of NH_4^+ to NO_3^- emissions in China[47], suggesting a strong linkage between emission sources from land and aerosol composition collected over the downwind oceanic regions. Overall, our synthesis reveals a pronounced shift in aerosol N_r sources between the NPSG and NPTZ, driven by distinct air-mass regimes, which largely govern aerosol N_r dynamics at the atmosphere-ocean boundary layer over the wNP.

Here, we obtain the basin-scale datasets of aerosol N_r deposition fluxes across the extensive wNP, derived from aerosol N_r concentrations and sinking velocities (see Methods). Because aerosol RN in the NPSG is predominantly marine in origin, it is excluded from our calculations; thus, our estimates represent external nitrogen inputs to the marine ecosystem. The resulting net aerosol N_r deposition fluxes exhibit significant spatial heterogeneity across subregions (Fig. 6a, see Methods for the subregional definition), with markedly higher annual mean fluxes in the Kuroshio and transition zones (47–110 μmol m^{-2} day^{-1}) compared to the central subtropical gyre (CSG) and the North Equatorial Current (NEC)-influenced region (5–13 μmol m^{-2} day^{-1}). This spatial pattern persists across all four seasons (Supplementary Table S4). Consistent with their proximity to East Asia, the Kuroshio and transition zones receive atmospheric N_r primarily from anthropogenic sources[33,37]. Therefore, we conclude that anthropogenic/terrestrial inputs dominate dry deposition for the extensive wNP, whereas natural sources prevail only in the NPSG.

Compared with regional N_2 fixation fluxes, pronounced contrasts in external nitrogen supply can be found among subregions (Fig. 6a). In the CSG and Kuroshio zone, both annual and seasonal mean N_2 fixation fluxes greatly exceed aerosol N_r deposition (Supplementary Table S4), reflecting the dominance of diazotroph-derived nitrogen inputs to these oligotrophic waters. In contrast, net aerosol N_r deposition fluxes in the NPTZ are ~1.5 times higher than N_2 fixation rates, consistent with suppressed diazotrophic activity under higher nutrient availability from atmospheric inputs and vertical mixing[43]. Both fluxes are low in the NEC-influenced region, likely due to weak terrestrial influence and enhanced subsurface nitrogen supply[42]. These patterns highlight regional differences in the relative importance of atmospheric and biological nitrogen sources in the wNP.

Distinct nutrient regimes among subregions may further regulate how external nitrogen is utilized. Unlike the N-limited oligotrophic CSG and Kuroshio zone, the NPTZ is non-N-limited (Fe-limited; Fig. 6b) and relatively mesotrophic, with moderately elevated surface Chl-a levels (0.1–0.8 mg m^{-3}; Fig. 1) and NO_3^- concentrations (0.4–5 μmol kg^{-1}), as indicated by observational and modeled results (Supplementary Fig. S6). In this regard, external nitrogen inputs may elevate the surface N_r inventory in the NPTZ and not promptly and effectively enhance primary and export production. By contrast, in those N-limited regions, external nitrogen inputs can rapidly stimulate primary and export production. We therefore propose that excess external nitrogen in the NPTZ can be laterally transported into the adjacent N-limited CSG, where it can fuel productivity. Indeed, such cross-frontal nutrient exchanges at the gyre margins along western boundary currents have been reported as an important pathway for replenishing nutrients and increasing biological productivity in the gyre interior[48].

Quantification of lateral transport of net aerosol N_r deposition and N_2 fixation signals above the mixed layer across subregions of the wNP confirms this mechanism. Based on the fluxes of external nitrogen inputs and the subregional water mass exchange rates (Fig. 6a; Supplementary Fig. S11; see Methods), we estimate that approximately 48% (46.5–49.6% seasonally) of external nitrogen inputs to the NPTZ are advected into the CSG; on an annual basis, this lateral transport supplies 16.7–20.9 μmol m^{-2} day^{-1} from aerosol N_r deposition and 12.1 μmol m^{-2} day^{-1} from N_2 fixation, with peak fluxes occurring in spring (Fig. 6b; Supplementary Table S5). These lateral fluxes are equivalent to 132–165% and 7% of the respective in situ inputs to the gyre, resulting in an overall ~18% (4–21% seasonally) increase in external nitrogen supply. When in situ and lateral advection fluxes are considered, external nitrogen sustains approximately 77% of annual export production in the CSG, based on the mean flux of ~273 μmol N m^{-2} day^{-1} at 100 m at time-series Station S1 (30°N, 145°E) measured using moored sediment traps (see Supplementary Table S5)[49,50]. Of this total, lateral ocean transport accounts for ~12%. Seasonally, the contribution of external nitrogen to export production is substantially greater during spring-summer (92-103%) than during autumn-winter (50-60%; Supplementary Table S5). In addition, it should be noted that our estimate is mainly focused on the surface water pathway. The subtropical and central mode waters formed in the NPTZ margin and, further east, are advected southwestward into the NPSG and subsequently subducted into the pycnocline[51]. This process may also facilitate cross-regional transport of external nutrients between these two subregions. However, the exact importance of this mechanism remains to be evaluated in future studies. Together, our results identify lateral ocean transport as a critical mechanism that amplifies the

influence of atmospheric nitrogen deposition on the subtropical gyre, highlighting the tight coupling between physical circulation and biogeochemical processes that shapes the overall productivity in the subtropical gyre ecosystem.

Methods

Aerosol and seawater collection

Samples for marine aerosol were collected from China's southeastern coast towards the North Pacific Subtropical Gyre (generally chlorophyll-a concentrations less than 0.1 mg m^{-3}) during summer (July to August 2020) and winter (December 2020 to February 2021; Fig. 1) using a high-volume air sampler (TE-5170D, TISCH Environmental, USA) placing on the top deck of the R/V *Tan Kah Kee* (~25 m above the sea surface). The sampler worked only during sailing to avoid contamination by the ship. We collected fifteen aerosol samples during each cruise using Whatman Grade 41 cellulose filters. The sampling duration for each sample was 24-96 hours, depending on the cruise path (Supplementary Table S1). Two filters for the field blank were sampled during each cruise. All filters were kept in clean, low-density polythene bags and stored at −20 °C before chemical and isotope analyses. Meteorological data, including wind speed, wind direction, air temperature, and relative humidity, were recorded using the automated weather station onboard (Supplementary Table S2). In addition, seawater samples were collected at 3–5 m of the sites where aerosol samples were collected using Niskin bottles during two cruises. Seawater samples for NH_4^+ measurements were analyzed onboard, and samples for other parameters were immediately stored at −20 °C until analysis.

Chemical and isotope analyses

The procedure for extracting total suspended particulate (TSP) samples followed Luo et al.[33]. In brief, a quarter of each filter was cut into pieces and placed in a centrifuge tube with 30 mL Milli-Q water. The fragmented filter was leached for 30 min on a shaker at 120 rpm and then left at room temperature for 30 min. The leaching processes were repeated three times. The extracts were filtered through 0.22 μm polycarbonate membranes. Major ionic species (Cl^-, NO_3^-, Na^+, and NH_4^+) in the extracts were analyzed using ion chromatographs (model ICS-900 for cations and model ICS-1100 for anions) equipped with a conductivity detector[28]. The detection limits for Cl^- and NH_4^+ were 0.015 mg L^{-1}, and for other ions were 0.010 mg L^{-1}.

Seawater nitrate concentration was analyzed using a continuous-flow analysis system combined with a liquid waveguide capillary flow cell, with a detection limit of 5.2 nmol L^{-1} and an analytical precision of 4.7%[52]. Seawater ammonium concentration was determined on board using solid-phase extraction coupled with a fluorescence detector, with a detection limit of 2.3 nmol L^{-1} and an analytical precision of 5.8%[53]. Chl-a in the surface seawater was extracted with acetone and measured using a Turner Trilogy fluorometer, and the data were reported in Zhang et al.[54].

The water-soluble total nitrogen in the aerosol extract (i.e., WSTN) and total dissolved nitrogen in the surface seawater (i.e., TDN) were determined using the 'persulfate oxidation' method to convert the total nitrogen to NO_3^-[55]. The NO_3^- was then measured by a nitrogen oxide (NO_x) chemiluminescence analyzer (Teledyne) with a detection limit of 10 nmol L^{-1}. Because the NO_3^- and NH_4^+ concentrations in the surface seawater of the study area were generally below 0.1 μmol L^{-1}, the measured TDN mainly consisted of dissolved organic nitrogen (DON; hereafter, TDN is reported as DON). The concentrations of water-soluble organic nitrogen ([WSON]) and reduced nitrogen ([RN]) in the aerosol extract were calculated using the following equations:

$$[\mathrm{WSON}] = [\mathrm{WSTN}] - [\mathrm{NH_4^+}] - [\mathrm{NO_3^-}] \quad (1)$$

$$[\mathrm{RN}] = [\mathrm{WSTN}] - [\mathrm{NO_3^-}] = [\mathrm{WSON}] + [\mathrm{NH_4^+}] \quad (2)$$

where $[NH_4^+]$ and $[NO_3^-]$ are the NH_4^+ and NO_3^- concentrations in the aerosol extract measured by ion chromatography.

N and O isotope compositions in NO_3^- (δ^{15}N-NO_3^- and δ^{18}O-NO_3^-) were analyzed using the denitrifier method[56,57]. Detailed information on the isotope analysis was reported by Yang et al.[28]. The measured δ^{15}N-NO_3^- values in the aerosol extract and seawater after the persulfate oxidation treatment represent the N isotope compositions of WSTN and DON (δ^{15}N-WSTN and δ^{15}N-DON), respectively. The standard deviations for replicates were ±0.2‰ for δ^{15}N-NO_3^-, ±0.3‰ for δ^{18}O-NO_3^-, and ±0.5‰ for δ^{15}N-WSTN and δ^{15}N-DON, respectively. The N isotope composition of RN (δ^{15}N-RN) in the aerosol extract was calculated based on mass and isotope balance, with a propagated error of ±0.6‰:

$$\delta^{15}\mathrm{N-RN} = (\delta^{15}\mathrm{N-WSTN} \times [\mathrm{WSTN}] - \delta^{15}\mathrm{N-NO_3^-} \times [\mathrm{NO_3^-}])/[\mathrm{RN}] \quad (3)$$

The concentration-weighted δ^{15}N value for each species was calculated using the following equation:

$$\delta^{15}N_{weighted} = \sum (C_i \times \delta^{15}N_i) / \sum C_i \quad (4)$$

where C_i and $\delta^{15}N_i$ represent the concentration and nitrogen isotopic composition for the given N_r species at each sampling site, respectively.

Calculation of atmospheric nitrogen deposition

We calculated the flux of atmospheric nitrogen deposition (F_i) according to the concentration of the given N_r species in aerosols (C_i) and the deposition velocity of the given N_r species (V_i), which is expressed as follows:

$$F_i = C_i \times V_i \quad (5)$$

As previous studies have suggested, V_i is influenced by many factors, such as meteorological conditions, particle size, and surface morphology, and thus varies widely[58]. For comparison with other works, we selected the V_i commonly used in the North Pacific, set to 2 cm s^{-1} for NO_3^-, 0.1 cm s^{-1} for NH_4^+, and 1.0 cm s^{-1} for WSON[33,59].

Backward trajectory analysis

A seven-day air mass backward trajectory (AMBT) was computed for each aerosol sample using the Hybrid Single-Particle Lagrangian Integrated Trajectory (HYSPLIT) model from the National Oceanic and Atmospheric Administration (NOAA; http://www.ready.noaa.gov/). The seven-day analysis corresponds to the average lifetime of aerosol nitrate, which is typically longer than that of aerosol RN under subtropical marine conditions[29]. Five altitudes (100, 250, 500, 1000, and 2000 m above ground level) were calculated to capture airflow transport into the marine boundary layer. Since the AMBTs were consistent among different altitudes, we present the 500 m height AMBTs as representative (Fig. 1).

Diagnosis of nutrient-limiting provinces

We diagnosed the spatial distribution of nutrient-limiting provinces for pico-phytoplankton, the dominant species in the study area, using annual mean fields from the ROMS-CoSiNE-Fe model[60]. Dissolved macronutrients (NO_3^-, NH_4^+, and PO_4^{3-}), dissolved iron (DFe) pools, and associated half-saturation constants were extracted at the surface model layer. For each nutrient *i*, the uptake rate was computed following the Michaelis-Menten formulation:

$$U_i = \frac{C_i}{K_i + C_i} \quad (6)$$

where C_i is the nutrient concentration and K_i is the corresponding half-saturation constant. The DFe field was computed as the sum of dissociated iron and iron complexed with strong and weak organic ligands.

Nitrate uptake additionally incorporated inhibition by ambient ammonium:

$$U_{NO_3} = e^{-\psi[NH_4]} \frac{[NO_3]}{K_{NO_3} + NO_3} \quad (7)$$

where ψ is the taxon-specific inhibition parameter.

Total potential N uptake was then given by:

$$U_N = U_{NO_3} + U_{NH_4} \quad (8)$$

At each horizontal grid cell, the limiting nutrient was identified as the one associated with the minimum potential uptake rate, following a standard Liebig minimum-law approach:

$$Lim = \min(U_N, U_{PO_4}, U_{DFe}) \quad (9)$$

The subregional definition and quantification of external nitrogen inputs transported by ocean circulation

The NEC-influenced region is defined as the main westward-flowing current that separates the tropical and subtropical circulations. By vertically integrating the zonal transport U over the upper 0–100 m, the $U = 0$ contour was used to delineate the dynamical boundary of the NEC. The NEC-influenced region is thus bounded by the northern boundary of the NEC and the southern boundary of the N-limited gyre. The Kuroshio region is defined as the western boundary current north of the NEC bifurcation latitude along the Philippine coast. The instantaneous axis of the Kuroshio was defined using the 0.7 m Sea Surface Height (SSH) contour. The analysis domain extends from the Philippine coast to 150 km east of the axis. This definition captures the main body of the Kuroshio while accounting for its meandering[61].

Lateral transport fluxes of external nitrogen signals from net aerosol N_r deposition and N_2 fixation from the transition zone to the central subtropical gyre via ocean circulation above the mixed layer were quantified using the observational flux datasets coupled with water mass flow rates simulated by the Regional Ocean Model System (ROMS). The model domain spans 45°S-65°N and 99°E-70°W, with a horizontal resolution of 1/8° (~12.5 km) and 60 sigma vertical layers. Vertical turbulent mixing is based on the Mellor-Yamada 2.5-level turbulence closure scheme. Using the 2002–2022 monthly climatological forcing fields, the model was forced by the reanalysis products of the European Center for Medium-Range Weather Forecasts (ERA5) for 30 years to reach a steady state. Then, we ran the real-time series from 2015 and used the data from 2017 for analysis. The model results were well validated in the Kuroshio Extension and in the NPSG[60,62].

The water transport fluxes of net aerosol N_r deposition or N_2 fixation signals per unit area received by the central subtropical gyre ($F_{transported}$, μmol m^{-2} day^{-1}) above the mixed layer were calculated as:

$$F_{transported} = \alpha \times F_{in} \times \frac{Q_i}{Q_{total}} \quad (10)$$

$$\alpha = \frac{A_{tz}}{A_{sg}} \times \frac{D_{tz}}{D_{sg}} \quad (11)$$

$$Q_i = \int_{-D}^{0} \int_{l_1}^{l_2} U_n(l, z)\, dldz \quad (12)$$

where A_{tz}/A_{sg} is the surface area ratio between the transition zone and the subtropical gyre the central subtropical gyre, and D_{tz}/D_{sg} refers to the mixed-layer depth ratio between the transition zone and the subtropical gyre (Supplementary Table S5). The mixed-layer depth data were obtained from the GLORYS12V1 global ocean reanalysis dataset[63]. Q_i and Q_{total} indicate the outflow rate of the corresponding section and the total outflow rate of each subregion, respectively. F_{in} shows the in situ flux of net aerosol N_r deposition or N_2 fixation. l_1 and l_2 denote the starting and ending outflow grid points of the section across subregions; A refers to the surface area of each subregion, and $U_n(l, z)$ represents the outflow velocity of each grid point.

Statistical analysis

The significance of differences among longitude and latitude groups was analyzed by one-way ANOVA, followed by Tukey tests. The relationships between the environmental variables and the aerosol data were examined using Student's t-test. All statistical analyses in this study were performed using Python 3.11.7. The significant differences are marked with asterisks ($^*p < 0.05$, $^{**}p < 0.01$, $^{***}p < 0.001$, $^{****}p < 0.0001$).

Data availability

The datasets generated and/or analyzed during the current study were deposited into the Zenodo repository[64] and are available at the following: https://doi.org/10.5281/zenodo.18871497.

Received: 5 January 2026; Accepted: 10 March 2026;
Published online: 25 March 2026

References

1. Browning, T. J. & Moore, C. M. Global analysis of ocean phytoplankton nutrient limitation reveals high prevalence of co-limitation. *Nat. Commun.* **14**, 5014 (2023).
2. Duce, R. A. et al. Impacts of atmospheric anthropogenic nitrogen on the open ocean. *Science* **320**, 893–897 (2008).
3. Gruber, N. & Galloway, J. N. An earth-system perspective of the global nitrogen cycle. *Nature* **451**, 293–296 (2008).
4. Jickells, T. D. et al. A reevaluation of the magnitude and impacts of anthropogenic atmospheric nitrogen inputs on the ocean. *Glob. Biogeochem. Cycles* **31**, 289–305 (2017).
5. Kim, T. W., Lee, K., Duce, R. & Liss, P. Impact of atmospheric nitrogen deposition on phytoplankton productivity in the South China Sea. *Geophys. Res. Lett.* **41**, 3156–3162 (2014).
6. Okin, G. S. et al. Impacts of atmospheric nutrient deposition on marine productivity: Roles of nitrogen, phosphorus, and iron. *Glob. Biogeochem. Cycles* **25**, GB2022 (2011).
7. Yang, J. Y. T. et al. Contrasting decadal trends of subsurface excess nitrate in the western and eastern North Atlantic Ocean. *Biogeosciences* **17**, 3631–3642 (2020).
8. Dai, M. et al. Upper ocean biogeochemistry of the oligotrophic North Pacific Subtropical Gyre: From nutrient sources to carbon export. *Rev. Geophys.* **61**, e2022RG000800 (2023).
9. Kim, T. W., Lee, K., Najjar, R. G., Jeong, H. D. & Jeon, H. J. Increasing N abundance in the northwestern Pacific Ocean due to atmospheric nitrogen deposition. *Science* **334**, 505–509 (2011).
10. Kim, I.-N. et al. Increasing anthropogenic nitrogen in the North Pacific Ocean. *Science* **346**, 1102–1106 (2014).
11. Palter, J. B., Marinov, I., Sarmiento, J. L. & Gruber, N. Large-scale, persistent nutrient fronts of the world ocean: impacts on biogeochemistry. In *Chemical Oceanography of Frontal Zones* (ed Belkin, I. M) (Springer Berlin Heidelberg, 2013).
12. Wenegrat, J. O. et al. Enhanced mixing across the gyre boundary at the Gulf Stream front. *Proc. Natl. Acad. Sci. USA* **117**, 17607–17614 (2020).
13. Jung, J. et al. Atmospheric dry deposition of water-soluble nitrogen to the subarctic western North Pacific Ocean during summer. *Atmosphere* **10**, 351 (2019).
14. Luo, L. et al. Nitrogen speciation in various types of aerosols in spring over the northwestern Pacific Ocean. *Atmos. Chem. Phys.* **16**, 325–341 (2016).
15. Martino, M. et al. Western Pacific atmospheric nutrient deposition fluxes, their impact on surface ocean productivity. *Glob. Biogeochem. Cycles* **28**, 712–728 (2014).

16. Zhang, J., Zhang, G. S., Bi, Y. F. & Liu, S. M. Nitrogen species in rainwater and aerosols of the Yellow and East China seas: Effects of the East Asian monsoon and anthropogenic emissions and relevance for the NW Pacific Ocean. *Glob. Biogeochem. Cycles* **25**, GB3020 (2011).
17. Jung, J., Furutani, H. & Uematsu, M. Atmospheric inorganic nitrogen in marine aerosol and precipitation and its deposition to the North and South Pacific Oceans. *J. Atmos. Chem.* **68**, 157–181 (2011).
18. Kamezaki, K. et al. Tracing the sources and formation pathways of atmospheric particulate nitrate over the Pacific Ocean using stable isotopes. *Atmos. Environ.* **209**, 152–166 (2019).
19. Lao, Q. et al. Hemispherical scale mechanisms of nitrate formation in global marine aerosols. *npj Clim. Atmos. Sci.* **7**, 139 (2024).
20. Miyazaki, Y., Kawamura, K., Jung, J., Furutani, H. & Uematsu, M. Latitudinal distributions of organic nitrogen and organic carbon in marine aerosols over the western North Pacific. *Atmos. Chem. Phys.* **11**, 3037–3049 (2011).
21. Violaki, K. et al. Atmospheric water-soluble organic nitrogen (WSON) over marine environments: a global perspective. *Biogeosciences* **12**, 3131–3140 (2015).
22. Zhao, Y. et al. Atmospheric nitrogen deposition to the northwestern Pacific: seasonal variation and source attribution. *Atmos. Chem. Phys.* **15**, 10905–10924 (2015).
23. Altieri, K. E., Fawcett, S. E. & Hastings, M. G. Reactive nitrogen cycling in the atmosphere and ocean. *Annu. Rev. Earth Planet. Sci.* **49**, 523–550 (2021).
24. Altieri, K. E., Hastings, M. G., Gobel, A. R., Peters, A. J. & Sigman, D. M. Isotopic composition of rainwater nitrate at Bermuda: the influence of air mass source and chemistry in the marine boundary layer. *J. Geophys. Res. Atmos.* **118**, 11304–11316 (2013).
25. Hastings, M. G., Sigman, D. M. & Lipschultz, F. Isotopic evidence for source changes of nitrate in rain at Bermuda. *J. Geophys. Res. Atmos.* **108**, 4790 (2003).
26. Morin, S. et al. Comprehensive isotopic composition of atmospheric nitrate in the Atlantic Ocean boundary layer from 65°S to 79°N. *J. Geophys. Res.* **114**, D05303 (2009).
27. Shi, G. et al. Using stable isotopes to distinguish atmospheric nitrate production and its contribution to the surface ocean across hemispheres. *Earth Planet. Sci. Lett.* **564**, 116914 (2021).
28. Yang, J. Y. T., Hsu, S. C., Dai, M. H., Hsiao, S. S. Y. & Kao, S. J. Isotopic composition of water-soluble nitrate in bulk atmospheric deposition at Dongsha Island: sources and implications of external N supply to the northern South China Sea. *Biogeosciences* **11**, 1833–1846 (2014).
29. Joyce, E. E., Balint, S. J. & Hastings, M. G. Isotopic evidence that alkyl nitrates are important to aerosol nitrate formation in the equatorial Pacific. *Geophys. Res. Lett.* **49**, e2022GL099960 (2022).
30. Altieri, K. E., Hastings, M. G., Peters, A. J., Oleynik, S. & Sigman, D. M. Isotopic evidence for a marine ammonium source in rainwater at Bermuda. *Glob. Biogeochem. Cycles* **28**, 1066–1080 (2014).
31. Lin, C. T., Jickells, T. D., Baker, A. R., Marca, A. & Johnson, M. T. Aerosol isotopic ammonium signatures over the remote Atlantic Ocean. *Atmos. Environ.* **133**, 165–169 (2016).
32. Altieri, K. E., Fawcett, S. E., Peters, A. J., Sigman, D. M. & Hastings, M. G. Marine biogenic source of atmospheric organic nitrogen in the subtropical North Atlantic. *Proc. Natl. Acad. Sci. USA* **113**, 925–930 (2016).
33. Luo, L. et al. Sources of reactive nitrogen in marine aerosol over the Northwest Pacific Ocean in spring. *Atmos. Chem. Phys.* **18**, 6207–6222 (2018).
34. Miyazaki, K. et al. Decadal changes in global surface NOx emissions from multi-constituent satellite data assimilation. *Atmos. Chem. Phys.* **17**, 807–837 (2017).
35. Shi, J., Gao, H., Qi, J., Zhang, J. & Yao, X. Sources, compositions, and distributions of water-soluble organic nitrogen in aerosols over the China Sea. *J. Geophys. Res. Atmos.* **115**, D17303 (2010).
36. Xiao, H.-W. et al. Use of isotopic compositions of nitrate in TSP to identify sources and chemistry in South China Sea. *Atmos. Environ.* **109**, 70–78 (2015).
37. Zhang, K., Liu, S., Wu, N. & Xu, W. Isotopic components and source analysis of inorganic nitrogen in coastal aerosols of the Yellow Sea. *Front. Mar. Sci.* **9**, 993160 (2022).
38. Alexander, B. et al. Global inorganic nitrate production mechanisms: comparison of a global model with nitrate isotope observations. *Atmos. Chem. Phys.* **20**, 3859–3877 (2020).
39. Fisher, J. A. et al. Methyl, Ethyl, and Propyl Nitrates: global distribution and impacts on reactive nitrogen in remote marine environments. *J. Geophys. Res. Atmos.* **123**, 12429–12451 (2018).
40. Miyazaki, K., Eskes, H. J., Sudo, K. & Zhang, C. Global lightning NO_x production estimated by an assimilation of multiple satellite data sets. *Atmos. Chem. Phys.* **14**, 3277–3305 (2014).
41. Dobashi, T. et al. Marine nitrogen fixation as a possible source of atmospheric water-soluble organic nitrogen aerosols in the subtropical North Pacific. *Biogeosciences* **20**, 439–449 (2023).
42. Wen, Z. et al. Nutrient regulation of biological nitrogen fixation across the tropical western North Pacific. *Sci. Adv.* **8**, eabl7564 (2022).
43. Shao, Z. et al. Global oceanic diazotroph database version 2 and elevated estimate of global oceanic N_2 fixation. *Earth Syst. Sci. Data* **15**, 3673–3709 (2023).
44. Jickells, T. D. et al. Isotopic evidence for a marine ammonia source. *Geophys. Res. Lett.* **30**, 1374 (2003).
45. Gobel, A. R., Altieri, K. E., Peters, A. J., Hastings, M. G. & Sigman, D. M. Insights into anthropogenic nitrogen deposition to the North Atlantic investigated using the isotopic composition of aerosol and rainwater nitrate. *Geophys. Res. Lett.* **40**, 5977–5982 (2013).
46. Savarino, J. et al. Isotopic composition of atmospheric nitrate in a tropical marine boundary layer. *Proc. Natl. Acad. Sci. USA* **110**, 17668–17673 (2013).
47. Liu, X. et al. Enhanced nitrogen deposition over China. *Nature* **494**, 459–462 (2013).
48. Letscher, R. T., Primeau, F. & Moore, J. K. Nutrient budgets in the subtropical ocean gyres dominated by lateral transport. *Nat. Geosci.* **9**, 815–819 (2016).
49. Mino, Y. et al. Seasonal and interannual variations in nitrogen availability and particle export in the Northwestern North Pacific Subtropical Gyre. *J. Geophys. Res. Oceans* **125**, e2019JC015600 (2020).
50. Honda, M. C. Effective vertical transport of particulate organic carbon in the Western North Pacific Subarctic Region. *Front. Earth Sci.* **8**, 366 (2020).
51. Oka, E. & Qiu, B. Progress of North Pacific mode water research in the past decade. *J. Oceanogr.* **68**, 5–20 (2012).
52. Zhang, J.-Z. Shipboard automated determination of trace concentrations of nitrite and nitrate in oligotrophic water by gas-segmented continuous flow analysis with a liquid waveguide capillary flow cell. *Deep Sea Res. Part I Oceanogr. Res. Pap.* **47**, 1157–1171 (2000).
53. Zhu, Y. et al. On the fluorometric measurement of ammonium in oligotrophic seawater: Assessment of reagent blanks and interferences. *Limnol. Oceanogr. Methods* **16**, 516–524 (2018).
54. Zhang, Y. et al. Decoupling of bacterial production and respiration in the surface water of the North Pacific Subtropical Gyre. *Mar. Life Sci. Technol.* **7**, 397–412 (2025).
55. Knapp, A. N., Sigman, D. M. & Lipschultz, F. N isotopic composition of dissolved organic nitrogen and nitrate at the Bermuda Atlantic Time-series Study site. *Glob. Biogeochem. Cycles* **19**, 17–33 (2005).
56. Casciotti, K. L., Sigman, D. M., Hastings, M. G., Bohlke, J. K. & Hilkert, A. Measurement of the oxygen isotopic composition of nitrate in seawater and freshwater using the denitrifier method. *Anal. Chem.* **74**, 4905–4912 (2002).

57. Sigman, D. M. et al. A bacterial method for the nitrogen isotopic analysis of nitrate in seawater and freshwater. *Anal. Chem.* **73**, 4145–4153 (2001).
58. Hoppel, W. A., Frick, G. M. & Fitzgerald, J. W. Surface source function for sea-salt aerosol and aerosol dry deposition to the ocean surface. *J. Geophys. Res. Atmos.* **107**, 4382 (2002).
59. Jung, J., Furutani, H., Uematsu, M., Kim, S. & Yoon, S. Atmospheric inorganic nitrogen input via dry, wet, and sea fog deposition to the subarctic western North Pacific Ocean. *Atmos. Chem. Phys.* **13**, 411–428 (2013).
60. Ma, W. et al. Contrasting supply dynamics of dissolved iron and nitrate shape the biogeography of nutrient-limiting conditions in the North Pacific. *Geophys. Res. Lett.* **51**, e2024GL111335 (2024).
61. Qiu, B. et al. The Pacific North Equatorial Current: new insights from the origins of the Kuroshio and Mindanao Currents (OKMC) Project. *Oceanography* **28**, 24–33 (2015).
62. Lin, P., Ma, J., Chai, F., Xiu, P. & Liu, H. Decadal variability of nutrients and biomass in the southern region of Kuroshio Extension. *Prog. Oceanogr.* **188**, 102441 (2020).
63. Jean-Michel, L. et al. The Copernicus Global 1/12° Oceanic and Sea Ice GLORYS12 Reanalysis. *Front. Earth Sci.* **9**, 698876 (2021).
64. Yang, J. Y. Datasets for aerosol nitrogen concentrations, N isotopic composition and fluxes in the western North Pacific Data sets. *Zenodo* https://doi.org/10.5281/zenodo.18871497 (2026).
65. Baker, A. R. et al. Observation- and model-based estimates of particulate dry nitrogen deposition to the oceans. *Atmos. Chem. Phys.* **17**, 8189–8210 (2017).
66. Seok, M.-W. et al. Atmospheric deposition of inorganic nutrients to the Western North Pacific Ocean. *Sci. Total Environ.* **793**, 148401 (2021).
67. Sato, T. et al. Revisiting the distribution and total amount of nitrogen fixation across the Kuroshio. *Limnol. Oceanogr. Lett.* **10**, 495–505 (2025).
68. Yu, X. et al. Assessing N2 fixation flux and its controlling factors in the (sub)tropical western North Pacific through high-resolution observations. *Limnol. Oceanogr. Lett.* **9**, 716–724 (2024).

Acknowledgements

We thank the captain and crew of the R/V Tan Kah Kee (Xiamen University) for their assistance at sea. We thank Li Tian, Wenbin Zou, Yutong Yang, Lifang Wang, Menghao Ma, and Tao Huang for their help with sampling and nutrient measurements. This work was supported by the National Key Research and Development Program of China (2023YFF0805001), the National Natural Science Foundation of China (42476032, 42330401, 42130401), and the Research Grants Council of the Hong Kong Special Administrative Region, China (No. AoE/P-601/23-N).

Author contributions

L.W. and D.D. analyzed the data and drafted the manuscript. J.Y.T.Y. designed this study and revised the manuscript. W.M., Z.Z., L.L., X.L., H.B., S.J.K., and M.D. discussed the results and contributed to the final manuscript.

Competing interests

The authors declare no competing interests.

Additional information

Supplementary information The online version contains supplementary material available at https://doi.org/10.1038/s41612-026-01388-7.

Correspondence and requests for materials should be addressed to Jin-Yu Terence Yang.